Special Collection

Peptidotriazolamers Inhibit Aβ(1–42) Oligomerization and Cross a Blood-Brain-Barrier Model

Nicolo Tonali[+],*[a, b] Loreen Hericks[+],[a] David C. Schröder,[a] Oliver Kracker,[a] Radosław Krzemieniecki,[a] Julia Kaffy,[b] Vadim Le Joncour,[c] Pirjo Laakkonen,[c] Antoine Marion,[d] Sandrine Ongeri,[b] Veronica I. Dodero,[a] and Norbert Sewald*[a]

In peptidotriazolamers every second peptide bond is replaced by a 1*H*-1,2,3-triazole. Such foldamers are expected to bridge the gap in molecular weight between small-molecule drugs and protein-based drugs. Amyloid β (Aβ) aggregates play an important role in Alzheimer's disease. We studied the impact of amide bond replacements by 1,4-disubstituted 1*H*-1,2,3-triazoles on the inhibitory activity of the aggregation "hot spots" $K^{16}LVFF^{20}$ and $G^{39}VVIA^{42}$ in Aβ(1–42). We found that peptidotriazolamers act as modulators of the Aβ(1–42) oligomerization. Some peptidotriazolamers are able to interfere with the formation of toxic early Aβ oligomers, depending on the position of the triazoles, which is also supported by computational studies. Preliminary in vitro results demonstrate that a highly active peptidotriazolamer is also able to cross the blood-brain-barrier.

Introduction

Degenerative disorders due to misfolding and assembly into various aggregate structures involve actually more than 30 human proteins leading to at least 20 serious human diseases, named amyloidoses.[1] Among them, Alzheimer's disease (AD) can be included as a calamitous neurodegenerative amyloidosis inducing progressive cognitive decline, functional impairment, and loss of independence.[2] The number of people worldwide suffering from AD is expected to reach 75 million by 2030, while no treatment is available to stop or even slow down the progression of the disease.[3] The approved drugs only provide symptomatic relief and short-term benefits. To date, the pathogenesis of AD is under debate. Besides the most widely accepted amyloid cascade[4] and cross-interaction[5,6] hypotheses, other assumptions were suggested: tauopathies, cholinergic neuron damage, oxidative stress, inflammation, microbiota influencing the immune and endocrine system, and genetic disposition.[2,7] According to the amyloid cascade hypothesis, amyloid β (Aβ) aggregates play an important role in the pathological progression of AD. Aβ spontaneously self-associates into soluble oligomers and insoluble aggregates like protofibrils and fibrils with high β-sheet content.[4] In the past 20 years, the Aβ plaques were considered the main target for therapeutic development and inhibitors of Aβ aggregation were designed to reduce the formation of insoluble fibers.[8] However, all therapeutics reaching phase III clinical trials failed so far, which led to questioning the role of Aβ and amyloid deposition in AD pathology.[9–11] Increasing evidence showed that the small and soluble Aβ oligomers rather than the insoluble aggregates are particularly cytotoxic and contribute to either neuronal death and/or affect synaptic neurotransmission.[12] This consideration allowed to reconsider the amyloid cascade hypothesis and underlines the early aggregation of Aβ to act as a critical trigger in the etiopathogenesis of the disease. Aβ oligomers are responsible for the disruption of the learning behavior in rats and that can also trigger events such as oxidative damage, inflammation, and calcium deregulation. Moreover, Aβ oligomers have been shown to also induce tau hyperphosphorylation, leading to neurite degeneration.[13,14] In this context, shifting treatment to a pre-symptomatic stage appears as an appealing and relevant alternative. Therapeutic strategies intervening at the early oligomerization process rather than at the later fibrillation step have indeed attracted attention recently.[15] Among the various strategies which have been adopted to stop or revert the progression of the disease, the modulation or inhibition of the aggregation process of Aβ has been approached through different mechanisms: stabilization of its native state,[16] bypassing the on-pathway oligomer

[a] *Dr. N. Tonali,[+] L. Hericks,[+] D. C. Schröder, O. Kracker, R. Krzemieniecki, Dr. V. I. Dodero, Prof. Dr. N. Sewald*
Organic and Bioorganic Chemistry
Department of Chemistry Bielefeld University
PO Box 100131, 33501 Bielefeld (Germany)
E-mail: norbert.sewald@uni-bielefeld.de
nicolo.tonali@universite-paris-saclay.fr
[b] *Dr. N. Tonali,[+] Dr. J. Kaffy, Prof. Dr. S. Ongeri*
BioCIS
CNRS, Université Paris Saclay
5 rue Jean-Baptiste Clément, 92296 Châtenay-Malabry (France)
E-mail: nicolo.tonali@universite-paris-saclay.fr
[c] *Dr. V. Le Joncour, Prof. Dr. P. Laakkonen*
Research Programs Unit, Translational Cancer Medicine Research Program
University of Helsinki
00014 Helsinki (Finland)
[d] *Assist. Prof. Dr. A. Marion*
Department of Chemistry
Middle East Technical University
06800 Ankara (Turkey)
[+] *These authors contributed equally to this work.*

Supporting information for this article is available on the WWW under https://doi.org/10.1002/cplu.202000814

formation, inhibition of the fibril elongation and disaggregation of the already formed amyloid aggregates.[17–20] Several natural polyphenols have been reported to exhibit potent inhibitory action on Aβ aggregation,[21] but none of them was able to demonstrate improvement in cognitive faculties and efficacy on disease regression during clinical trials.[22] Generally, the main challenge in inhibiting protein-protein interactions is the modulation of large and relatively flexible surface areas.[23] The lack of affinity and selectivity of small molecules, when employed to modulate this type of interactions, is often related to this problem.

Aducanumab is a promising monoclonal antibody that is currently under consideration for approval by the FDA and EMA. It holds potential for becoming the first treatment for reducing clinical decline in AD owing to its ability to target both forms of Aβ, i.e., soluble oligomers and insoluble fibrils.[24,25] A major drawback of monoclonal antibodies is, however, the need for repeated administrations and the associated cost of production.[26]

Research in the protein-protein interaction field has been also oriented towards peptides, because they offer several advantages such as greater efficacy, specificity and selectivity, owing to their intermediate size between small molecule drugs and protein therapeutics.[27,28] Moreover, the risk of complication caused by their metabolites is reduced, thus making them safer.

Recently, we reported a new BODIPY-based real-time assay suitable for 96-well plate format that allows screening of compounds as selective inhibitors of the formation of Aβ(1–42) oligomers.[17] We were able to discover new active peptide inhibitors of the early oligomerization of Aβ(1–42). These peptides were derived from the two Aβ(1–42) aggregation "hot spots" $K^{16}LVFF^{20}$ and $G^{38}VVIA^{42}$, which form the hydrophobic central core and the *C*-terminal domain, respectively. The all-D-configured acetylated analog Ac-klvff-NH_2 **1** (Figure 1) proved to be able to interfere with both oligomerization and fibrillization, while the *C*-terminal fragment H-GVVIA-NH_2 **2** (Figure 1) proved to be a specific inhibitor of the oligomerization. Both **1** and **2**, therefore, show an ability to protect cells from cytotoxic Aβ(1–42) oligomers. Despite their effectiveness, the L-configured peptides are generally sensitive to proteolytic degradation and lack a specific secondary conformation, which might increase their affinity and specificity for Aβ(1–42).

Over the past decade, foldamers have increasingly attracted attention as useful tools to mimic secondary structures of proteins and peptides. Bio-inspired synthetic foldamers provide effective biopolymer mimics with new and improved physiological properties, and represent useful tools for practical applications in the areas of diagnostics or therapeutics.[29,30] Peptidomimetic foldamers offer the possibility to adopt secondary structures frequently involved in protein-protein interactions by maintaining at the same time the specific side chains of a peptide sequence.[31–33] In this regard, peptidomimetic foldamers represent a pharmacologically important class of compounds, as they are inspired by the structural features of their bioactive peptide counterparts. Some of us have already demonstrated that peptidomimetic foldamers are able to inhibit more efficiently the amyloid aggregation and to preserve the non-toxic monomer species, thanks to their preorganization as β-hairpins[18,19,34] or α-helices.[35]

Inspired by the triazolamers pioneered by the Arora workgroup,[36] which showed encouraging results as protease inhibitors, the synthesis of a new class of peptidomimetics containing 1,4- or 1,5-disubstituted 1*H*-1,2,3-triazoles and amide bonds in an alternating fashion was reported by us.[37,38] These peptidomimetics, which were named peptidotriazolamers, can be considered as hybrid foldamers with features of peptides and triazolamers, with conservation of the amino acid side chain. In 2014, Johansson *et al.* described the synthesis of several achiral peptidotriazolamers of various lengths, comprising 1,5-disubstituted triazoles and peptide bonds in an alternating pattern.[39] Their conformational analysis and quantum chemical calculations showed the concurrence of various conformers with comparable stabilities.[39] Based on new synthetic approaches toward enantiomerically pure propargylamines with stereogenic centers in the propargylic position, we reported on synthesis and conformational analysis of homo- or heterochiral peptidotriazolamers.[37,38] In the case of 1,5-disubstituted peptidotriazolamers the homochiral analog forms a compact β-turn-like structure, while the heterochiral one with alternating chirality adopts a polyproline I-like conformation.[37] Investigation of conformational properties of 1,4-disubstituted peptidotriazolamers by molecular dynamics simulations, using specifically tailored force field parameters, suggested a well-defined and significantly different secondary structure for the homo- (helix) and heterochiral (twisted S) variants in DMSO.[38]

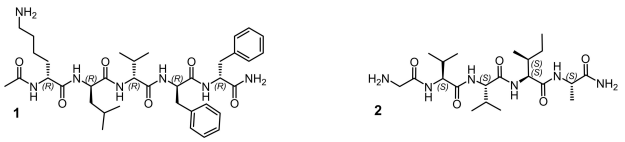

Figure 1. Parent peptides Ac-klvff-NH_2 **1** and H-GVVIA-NH_2 **2**.[17]

Results and Discussion

In the present study, we investigated the potential application of 1,4-disubstituted peptidotriazolamers for the design of new inhibitors of Aβ(1–42) oligomerization. In particular, the impact of the amide bond substitution by 1,4-disubstituted 1*H*-1,2,3-triazoles on the inhibitory activity of the two "hot spots" $K^{16}LVFF^{20}$ and $G^{39}VVIA^{42}$ was of interest. These sequences correspond to the previously described peptides **1** and **2** (Figure 1).[17]

We substituted two amide bonds in both sequences in an alternating fashion and thus obtained five new peptidomimetics **3**–**7** (Figure 2): **3**, **4**, and **6** with the substitution at the second and fourth amide bonds, while **5** and **7** at the first and third ones. The two $K^{16}LVFF^{20}$ peptidotriazolamers **3** and **4**, with L- and D-configuration respectively, were designed in order to evaluate the possible influence of the stereochemistry on the inhibitory activity. These new compounds were assessed in the complementary ThT and BODIPY fluorescence assays and in a

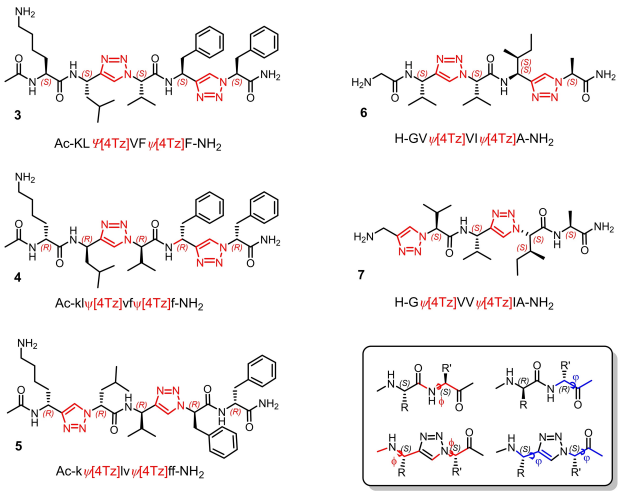

Figure 2. Chemical structure of the five peptidotriazolamers **3**–**7** discussed in this study.

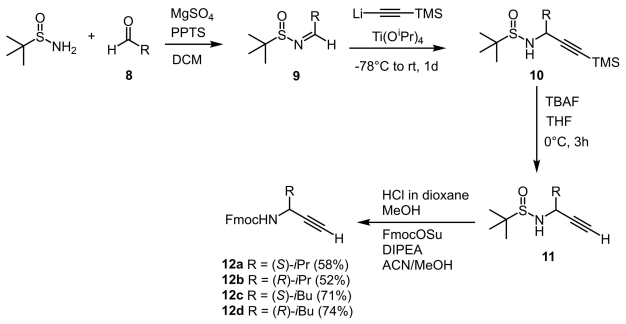

Scheme 1. Synthesis of propargylamines **12a**–**d** using Ellman's auxiliary.

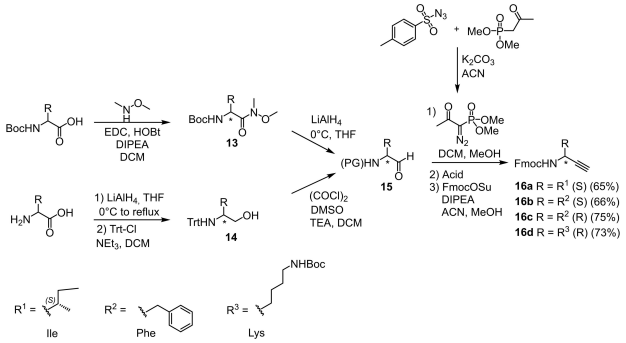

Scheme 2. Synthesis of propargylamines **16a**–**d** according to the Bestmann-Ohira approach.

cell viability assay in order to evaluate their ability to maintain or even improve the inhibitor activity on the fibrillization and/or oligomerization of Aβ(1–42), as their peptide counterparts. This structure-activity relationship study together with molecular dynamics simulations allowed us to identify the best position for the triazole rings in the peptide sequence and the conformational secondary structure requirement to modulate the protein-protein interactions. Finally, we investigated the ability of the best peptidotriazolamer to cross the blood-brain-barrier (BBB) to assess its potential use *in vivo*.

Synthesis

Peptidotriazolamers **3**–**7** were synthesized by employing a building block strategy where the triazole is formed from the propargylamine and the azide by copper-catalyzed azide-alkyne cycloaddition (CuAAC) and then coupled by amide bond formation in solid phase peptide synthesis (SPPS).[40]

Triazoles substituted with adjacent stereogenic centres require enantiomerically pure propargylamines and α-azido acids.[41] The *(S)*– or *(R)*– configured propargylamines, bearing the Val (**12a,b**) and Leu (**12c,d**) side chains, were obtained using Ellman's auxiliary as described by Wünsch et al.[42] (Scheme 1), while the *(S)*– or *(R)*–configured propargylamines **16a**–**d** bearing the Ile, Phe and Lys side chains, are accessible by Bestmann-Ohira reaction (Scheme 2). In the Ellman's auxiliary approach, condensation of the corresponding aldehydes **8** with *(S)*- or *(R)*-configured tert-butyl sulfinamide led to the enantiomerically pure sulfinylimines **9**, which were reacted with (trimethylsilyl)ethynyllithium, to give the intermediates **10**. The terminal TMS group was successively cleaved to provide the Bus- (*tert*-butyl sulfinyl) protected propargylamines **11**, with satisfactory yields (50-60%) and a diastereomeric ratio of 97:3. The Bus group was then replaced by Fmoc as required for SPPS (Scheme 1).

In the Bestmann-Ohira approach, the carboxylic acid of the *(S)*- or *(R)*-Phe and Lys was first reduced to the alcohol **14** (80-90% of yield for Phe and 40% for Lys) (Scheme 2), which subsequently was oxidized in a Swern oxidation to give the corresponding aldehydes **15**, which were used without further purification for the next step. The latter was then converted into the propargylamines (**16b**–**d**) using the Bestmann-Ohira reagent (yields over two steps of 80% for Phe and 53% for Lys). For propargylamine **16a**, the aldehyde was obtained by reduction of the Weinreb amide **13** (Scheme 2) by $LiAlH_4$. The acid labile Boc or Trityl groups were successively cleaved and replaced by Fmoc to obtain the final propargylamines (**16a**–**d**), suitable for SPPS.

The synthesis of chiral α-azidoesters (**18a**–**g**, Scheme 3) preferably makes use of the pool of naturally occurring amino acids that can be converted employing Wong's procedure, using Cu^{II}-catalysed diazo transfer from triflyl azide.[43] The azides were synthesized in excellent yields of >87%, starting from the corresponding commercially available amino acid benzyl ester salts.

Triazole formation was achieved by CuAAC in the presence of $CuSO_4 \cdot 5H_2O$ (1.2 eq) and sodium ascorbate (2.4 eq) in *t*BuOH/H_2O mixture to afford ten 1,4-disubstituted 1*H*-1,2,3-triazoles (compounds **19a**–**j**) as dipeptide mimetic building blocks with satisfactory yields (40-90%) (Scheme 3). Afterwards the benzyl ester was hydrogenolyzed with triethylsilane in methanol to obtain the corresponding intermediates (**20a**–**j**) suitable for SPPS (Scheme 3). The peptidomimetics **3**–**7** were assembled according to the building block strategy in SPPS by

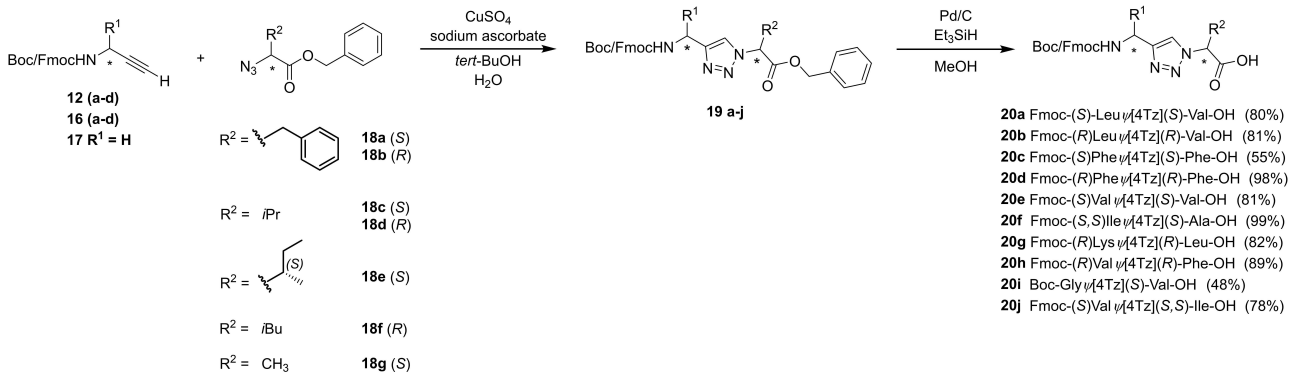

Scheme 3. Synthesis of the dipeptide peptidotriazolamers (**20 a–j**) according to the Bestmann-Ohira approach.

employing Rink amide resin as solid support in order to install a carboxamide at the *C*-terminus.

A general synthetic scheme of the peptidotriazolamer is given in Scheme 4. The dipeptide building blocks or the amino acid were loaded on the resin by using DIC/Oxyma and collidine in a mixture of DCM and DMF. After Fmoc removal, the dipeptide intermediate was coupled under the same conditions. For the peptidotriazolamers having the natural amino acid at the *N*-terminus (D- or L-Lys for **3** and **4** and Gly for **6**), the final amino acid was also coupled by using DIC/Oxyma and collidine.

Peptidomimetics **3**, **4**, and **5** were acetylated at the *N*-terminus before cleavage from resin, while for foldamers **6** and **7** the free *N*-terminal amine was afforded by directly removing the Boc *N*-protecting group under the acidic cleavage protocol. All peptidotriazolamers, **3**–**5** as KLVFF mimetics and **6** and **7** as GVVIA mimetics, were obtained in moderate to good yields after purification by reverse-phase HPLC.

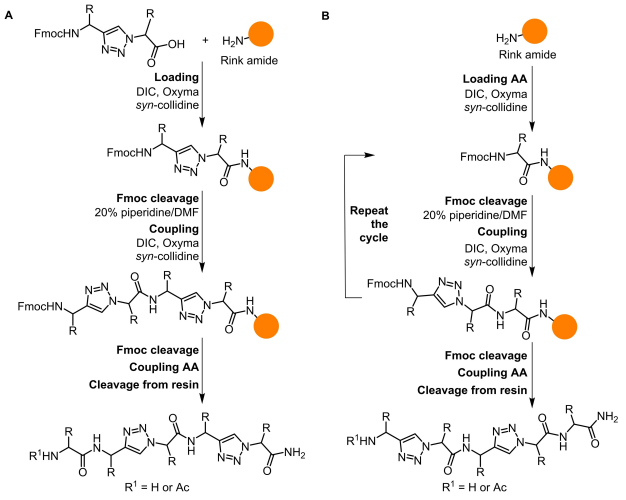

Scheme 4. General synthetic scheme for the SPPS of the peptidotriazolamers **3**, **4** and **6** (A) and for **5** and **7** (B), employing the building block strategy.

Fluorescence spectroscopy assays

Three calculated parameters from the BODIPY- and the ThT-fluorescence kinetic curves can be used to compare the activity of the inhibitors: $t_{1/2}$, which is defined as the time at which the fluorescence has reached 50% of its maximum (as a measure of the process rate), the slope of the elongation phase of the curve in the first 4 h of the BODIPY kinetics (as a measure of the process rate), and *F*, which is the fluorescence value of the final plateau and is assumed to depend on the number of aggregates and fibrils formed, respectively for the BODIPY and the ThT experiment.[17] Each parameter is defined as the experimental result in the presence of the tested compound relative to the one obtained without the compound and is evaluated as percentage. The presence of oligomers under the measurement conditions of the BODIPY fluorescence assay has been already demonstrated by various biophysical assays in our previous work.[17]

In the ThT assay, the five peptidotriazolamers **3**–**7** displayed modest to no inhibitory activity on the fibrillization process (Figure 3, A, C and E, and Figures S16–20 in the Supporting Information). In particular, in the KLVFF series the $t_{1/2}$ values as a measure of the fibrillization rate in the presence of **3**, **4**, and **5** ($-47\% < t_{1/2} < 14\%$) were lower than $t_{1/2}$ of the parent peptide **1**, which significantly delayed fibril formation ($t_{1/2=} + 154\%$, Table 1 and S1). Although the parent peptide **2** in the GVVIA series was inactive on fibril formation, replacing the second and the fourth amide bound by a triazole ring resulted in the potent inhibitor **6** of the fibrillization process. The rate was increased by 50% and the plateau decreased by 52% for **6** at compound/Aβ(1–42) ratio of 10/1 (Table S1 and Figure 3 C). This effect was maintained on the fluorescence plateau at a **6**/Aβ(1–42) ratio of 1/1 ($\Delta F_{=} -39\%$). However, this inhibitory effect was not observed for analogue **7** (Figure 3, E), bearing the triazole rings in the first and third amide bonds position, suggesting that these positions are critical for inhibition of fibril formation.

The BODIPY fluorescence assay revealed that all designed peptidotriazolamers (**3**–**7**) interfere with early oligomer formation (Table 1 and S1). Concerning the peptidotriazolamers based on the KLVFF sequence, the substitution of two amide bonds by a triazole ring in the second and fourth positions (**3**

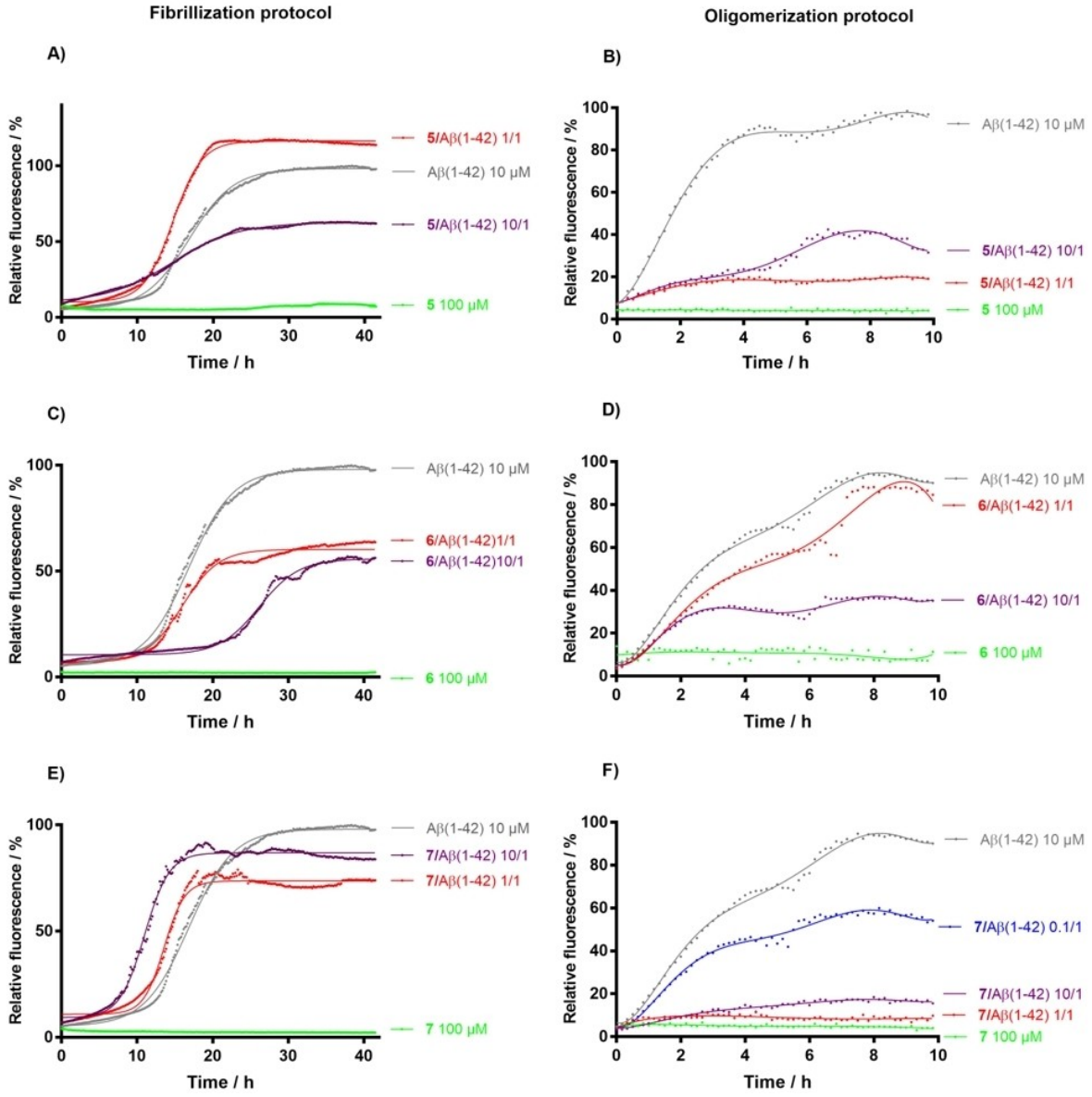

Figure 3. Time course of ThT and BODIPY fluorescence showing Aβ(1–42) (10 μM) fibrilliization (A), (C), (E) and oligomerization (B), (D), (F) in the absence (grey curves) and in the presence of compounds **5** (A) and (B), **6** (C) and (D) and **7** (E) and (F) at compound/Aβ(1–42) ratios of 10/1 (purple curves) and 1/1 (red curves) and 0.1/1 (blue curve, only for compound **7** in the oligomerization assay). The curves are provided as the average curves of a triplicate.

Table 1. Effects of compounds **3**–**7** at compound/Aβ(1–42) ratio of 1:1 on 10 μM Aβ(1–42) fibril formation and oligomerization, as assessed by ThT- and BODIPY-fluorescence spectroscopy, respectively.[a]

Compound [compound/Aβ ratio]	ThT assay *F* extension/reduction [%]	$t_{1/2}$ extension/reduction [%]	BODIPY assay *F* reduction [%]	Slope reduction [%]
1	n.e.	+154±23	−84±0.4	−94±0.4
2	n.e.	n.e.	−80±0.3	−9±0.8
3	−19±2.7	−47±9.8	−43±1.8	−37±0.6
4	+27±11	−36±12.6	−20±0.6	−16±1.3
5	+32±17.8	−14±6.7	−81±1.2	−88±0.4
6	−39±6.6	−9±0.4	−15±2.9	−14±0.4
7	n.e.	−24±5.7	−88±1.0	−93±0.4

[a] All the compounds were compared with the values obtained for Aβ(1–42) alone ($t_{1/2}$, F, and slope) and the ones for compounds **1** and **2**, already published in Tonali et al.[17] Parameters are calculated from the expressed as mean curves, as derived by statistical analysis of data after triplicate measurements for each condition and at least two independent experiments. n.e.: no effect (For further details about calculation, see the Supporting Information).

and **4**) resulted in a reduced inhibitory activity at equimolar ratio (compound/Aβ(1–42) 1:1) compared to the parent peptide **1**. Compounds **3**, **4** and **5** showed very good and similar efficacy at the highest ratio compound:Aβ(1–42) of 10:1 (Figure S21-S23). Compound **3**, with all-(*S*)-configuration and triazoles replacing the second and fourth amide bond positions, showed to be more effective in reducing the oligomerization rate at a compound/Aβ(1–42) ratio of 1:1 than the all-(*R*)-configured analog **4** (−37% for **3**, −16% for **4**, Table 1) as well as the amount of soluble oligomers (−43% for **3**, −20% for **4**) (Table 1, Figure S21–22). The positioning of the triazole rings as substitutes of the second and fourth amide bonds seems to require an inversion of the stereochemistry, compared to the peptide **1**, to maintain the activity. However, keeping the (*R*)-configuration and "shifting" the triazole position to the first and third amide bonds as in compound **5** resulted in an increase of the inhibitory effect (−88% of oligomerization rate reduction and −81% of fluorescence decrease at a ratio 1:1, Table 1), suggesting a possible role of the triazole ring on the conformational behavior of the peptidotriazolamer (Figure 3, B). The same observation could be made for the foldamers based on the Aβ(1–42) *C*-terminal sequence (GVVIA): compound **7** (Figure 3, F) is, in fact, more active compared to **6** (Figure 3, D) and is able to inhibit the oligomerization process of Aβ(1–42) at both 10:1 and 1:1 ratio (−93% of oligomerization rate reduction and −88% of fluorescence decrease at ratio 1:1, Table 1), like its peptide counterpart **2**. Interestingly, compound **7** maintained a good inhibitory activity even at substoichiometric ratio (0.1:1) (Figure 3, F), suggesting an important role of the peptidotriazolamer in stabilizing the correct and necessary conformation for the interaction with the amyloid peptide, particularly when triazoles are in place of the first and the third peptide bonds in a pentapeptide sequence.

Cell viability assays

The most active compounds in the oligomerization assay, **5** and **7**, were tested in an MTS viability assay to confirm the effective rescue of SH-SY5Y neuroblastoma cells in the presence of toxic Aβ(1–42) oligomers. Their activities were compared to the one of a previously published *N*-acetylated peptide (Ac-GVVIA-NH_2) which is active only at a 5:1 ratio, but its protective effect is lost at equimolar ratio (1:1), thus behaving as positive and negative control at the same time.[17] Compounds **5** and **7** did not show any toxicity when incubated alone with cells at 25 μM concentration (Figure 4). The addition of compound **7** showed a significant protective effect on the cells from cytotoxic Aβ(1–42) oligomers at both equimolar and substoichiometric ratios, while compound **5** was significantly effective at both 5:1 and 1:1 ratios (**5**/Aβ(1–42)) (Figure 4). These results demonstrate that the replacement of the first and third amide bonds in the "hot spot" sequences of Aβ(1–42) is an efficient bioisosterism strategy to obtain new peptidomimetics with comparable activity. Moreover, the substoichiometric inhibitory activity of **7** compared to **5** proved that peptidotriazolamers, designed for the *C*-terminal sequence instead of the hydrophobic core of Aβ(1–42), are superior in inhibiting the formation of toxic early oligomers.

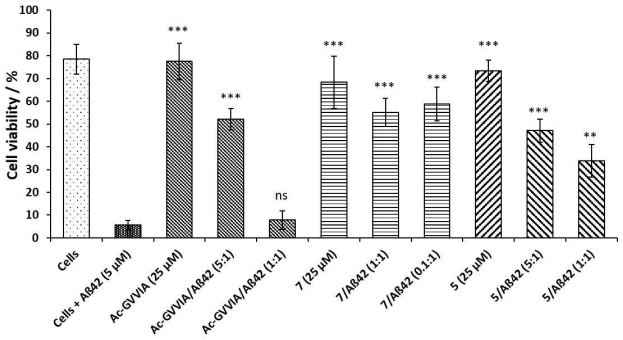

Figure 4. Cell viability assay results, representing the percentage of survival observed for cells incubated without Aβ(1–42), with only inhibitors (25 μM), and with 5 μm Aβ(1–42) with or without the different inhibitors at different ratio. A statistically significant difference to Aβ(1–42) treated cells is indicated by * $p < 0.05$, ** $p < 0.01$, and *** $p < 0.001$; $n = 6$ for each condition.

No concentration dependence of effects between 1:1 and 0.1:1 ratios for compound **7** has been found, thus suggesting that the slight perturbation of the oligomerization process at 0.1:1 ratio observed in the BODIPY assay (Fig. 3F, blue curve) is enough to produce a protective effect against Aβ(1–42) toxicity similar to the 1:1 ratio. Further studies will be necessary to explain the mechanism of action.

Conformational analysis

The conformational preferences of compounds **2**, **6**, and **7** were investigated by means of molecular dynamics (MD) simulations in explicit solvent, to shed light on the differences in activity observed experimentally and on the related impact of the triazole positioning in the GVVIA sequence. Following the strategy designed for our previous studies on peptidotriazolamers,[37,38] we used a tailored set of molecular mechanics parameters[44] and obtained the starting structures of MD simulations by performing a series of gas phase simulated annealing (SA) conformational samplings with NMR-derived NOESY interproton distance restraints. Restraints were then released, and simulations were performed in DMSO to address the validity of our models with respect to NMR results and in water to emulate a more biologically relevant environment. In both solvents, the *N*-terminal amine was modelled as protonated, with a trifluoracetate (TFA) or a chloride counterion for DMSO or water simulations, respectively, since the compound was obtained as a TFA salt and analyzed as such in NMR experiments. All 200 ns MD simulations were repeated three times to increase convergence of the results. Additionally, the same methodology was applied to a set of starting structures obtained from SA sampling without any interproton distance restraints. Both approaches yielded similar results, suggesting convergence of the conformational sampling and all results are reported in the Supporting Information. In the following, we

shall only focus on results obtained from MD run with NMR-based SA starting structures.

Analysis of the root mean square deviation (RMSD) and radius of gyration (RoG) time series (Figure S26) suggest that the simulations reached equilibrium and that the conformational sampling converged for all molecules. In general, the backbone of each compound is mainly responsible for the fluctuations of RMSD in both solvents. The natural peptide **2** and to some extent the peptidotriazolamer **7** have a more flexible backbone compared to compound **6** in both solvents. For each compound, there is no significant difference in the RMSD and RoG time series when moving from one solvent to another, expect for compound **2**, which seems to adopt a slightly more extended conformation in water when comparing its DMSO and water RoG time series.

Distributions of Φ/Ψ torsion angles pairs are depicted in the Supporting Information (Figure S27). Although a direct comparison of dihedral angles is not applicable when dealing with natural and modified peptides due to the differences in torsion angle definitions, a qualitative analysis of the conformations on a single amino acid basis reflects significant differences between the compounds. While each amino acid in the native peptide **2** populates two to three conformations on the Ramachandran plots, the introduction of triazole rings peptide bond isostere significantly rigidifies the backbone of compounds **6** and **7**. Consistently with the analysis of RMSD and RoG time series, the nature of the solvent has little to no effect on the conformational distribution of the three compounds.

Structural clustering based on backbone RMSD was performed to extract representative conformations of the three compounds (Figure 5) and to examine the impact of the amide bond isostere on the backbone conformation. The main clusters of all compounds were found to be highly stable with populations ranging from 48 to 99% in DMSO and from 74 to 81% in water. In the upper panel of Figure 5, the individual overlay of DMSO and water representative structures for each compound confirms the low impact of the solvent on the preferred conformation. Compounds **2** and **7** adopt a similar, extended conformation, while peptidotriazolamer **6** folds in a "U"-shape. Interproton distances derived from NMR spectra were compared with those measured over all frames of the major cluster in DMSO. For all three molecules, average deviations considering all interproton distances were found to be as small as 0.8 Å, which validates the predicted models

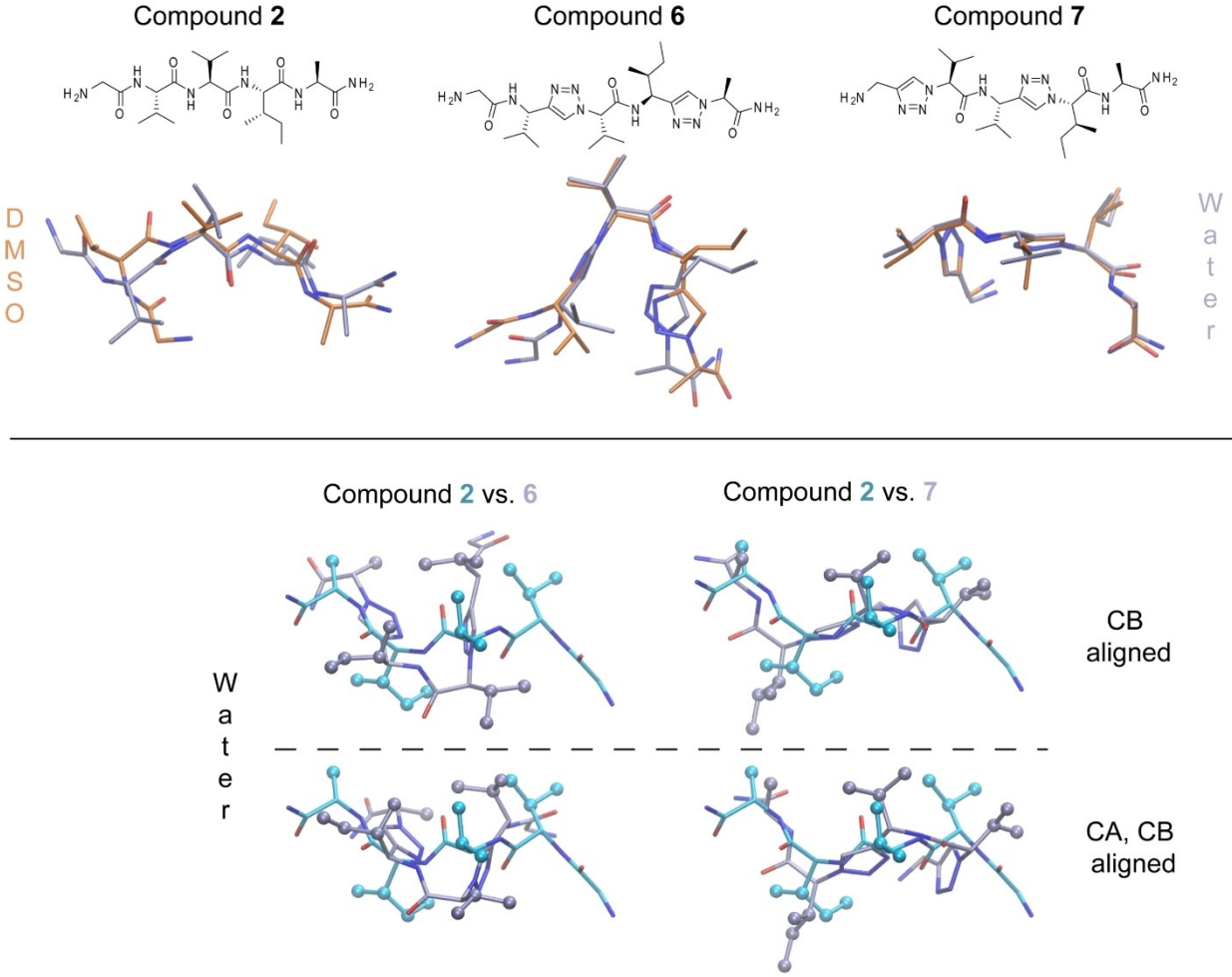

Figure 5. Upper panel: representative structures for the major backbone cluster of compounds **2**, **6** and **7** in DMSO (orange) and Water (iceblue); lower panel: superimposition of the representative structure of compounds **2** and **6** as well as **2** and **7** in water.

against experimental observations. The major deviations were associated with distance pairs involving hydrogen atoms in sidechains. A detailed analysis is available in Table S2. The similarities between **2** and **7** extend to the spatial orientation of their hydrophobic side chains, which overlap well except for the *N*-terminal part, resulting a similar signature for intermolecular interactions. On the contrary, compound **6** presents a significantly different spatial organization of its polar and non-polar chemical functions.

Solute-water radial distribution functions (RDFs) are depicted in Figure 6 for four selected atomic centers on the solute backbone. In all molecules, the glycine amino proton interacts with one water molecule yielding a characteristic peak for a hydrogen bond centered at about 1.8 Å. The triazole nitrogens N2 and N3 can serve as hydrogen bond acceptors and the corresponding distributions indeed peak at about 2.0 Å. However, as already pointed out in our previous studies on 1,4-peptidotriazoles,[38] the peak of the first solvation shell is broad and very low in intensity, indicating that the solvent is loosely interacting with these peptide bond surrogates. The RDF of the amine proton of alanine shows a sharp peak at 1.8 Å.

This peak integrates for one water molecules in the case of compound **2** and **7**, and for a substantially smaller fraction for compound **6**, indicating that the *N*-terminal part of the latter is somewhat less solvated than that of the two other molecules. Overall, even for the strongest interactions discussed for the three molecules, the RDF plots are characteristic of compounds with a significant hydrophobic character. This is in line with Lipinski's rule of five and its requirement for a certain degree of lipophilicity, which may be beneficial to promote the BBB passage of the present drug candidates.

Tran *et al.* had identified, via extensive replica exchange molecular dynamics, a structure of Aβ(1–42) that promotes oligomerization.[45] This structure, named *cluster03b* by the authors, was shown to form penta- and hexamers that remain stable over long MD simulation times. Figure 7B presents the main conformation of compounds **2**, **6**, and **7** obtained in water aligned to the *N*-terminal part of Aβ(1–42) according to Tran *et al.* As illustrated in the panel A of Figure 7, $G^{38}VVIA^{42}$ is involved in a β-sheet conformation that allows an exact match of hydrophobic side chains with the rest of the sequence and that contributes to the overall stability of the structure. Alignment of **2**, **6**, and **7** to $G^{38}VVIA^{42}$ shows that **2** and **7** can recapitulate both the conformation and the lipophilic signature of the *C*-terminal fragment of Aβ(1–42). Compound **6**, however, yields a very poor alignment due to its bent conformation.

This last observation is in line with the experimental BODIPY assay (Table 1) and highlights the similarities between compounds **2** and **7**. It also suggests a rationale for the significantly lower activity of compound **6** obtained in the assay. The intrinsically extended conformation of compounds **2** and **7** allows them to readily substitute $G^{38}VVIA^{42}$ in the oligomer forms of Aβ(1–42), while **6** adopts a conformation in solution that is incompatible. Compound **6** would need to undergo a significant conformational change in order to bind in place of $G^{38}VVIA^{42}$. Considering the high stability of the most populated structures for all three compounds in water, it can be inferred that such conformational change would be energetically demanding, which would prevent binding of **6** or significantly slow it down compared to **2** and **7**.

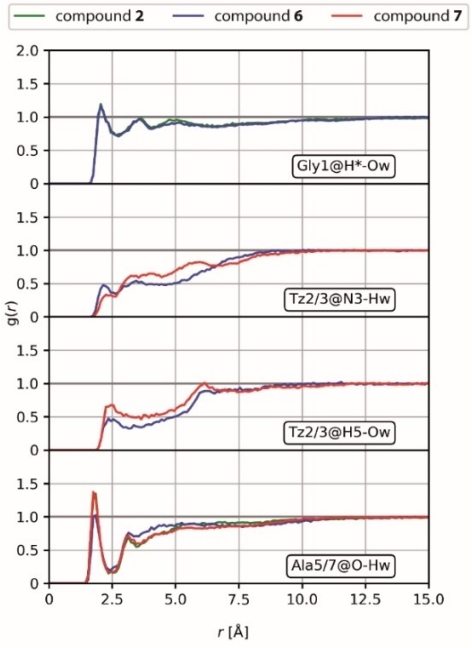

Figure 6. Radial distribution function for selected solute-water interactions.

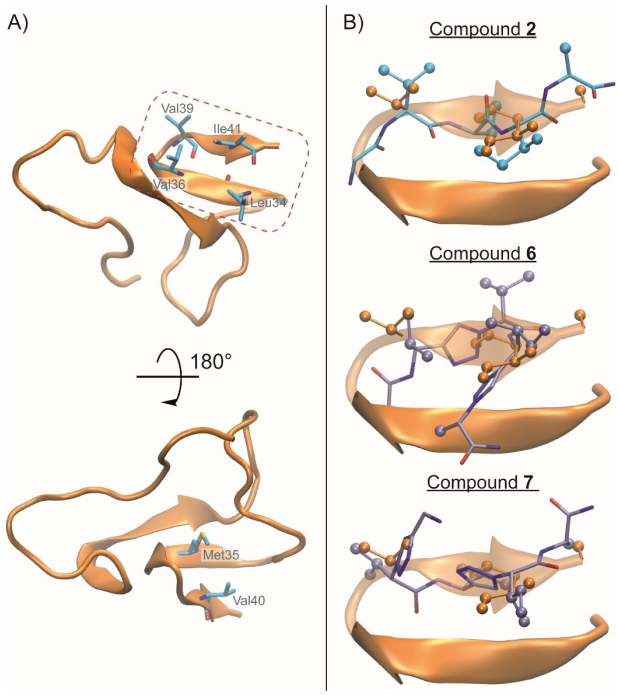

Figure 7. Possible mode of action of compounds **2** and **7** as aggregation inhibitor. A) Ring shaped 42 residue beta amyloid monomer (cluster03b from Tran *et al.*).[45] Beside the overall structures depicted in cartoon style, relevant side chains and backbone atoms stabilizing the β-sheet are highlighted in liquorice style. B) RMSD based structural alignment of compounds **2** (top), **6** (middle) and **7** (bottom), depicted in liquorice style, to the GVVIA-sequence, shown in cartoon style. The hydrophobic groups are depicted in CPK style.

In vitro blood-brain-barrier permeability measurements

Encouraged by the solute-water RDF results, we investigated the *in vitro* permeability of peptidotriazolamer **7**, the most active compound of the series, in order to evaluate its ability to cross an *in vitro* artificial blood-brain-barrier (aBBB). As quantified by HPLC-MS, **7** was found to cross the artificial BBB,[46] consisting of murine brain microcapillary or immortalized human umbilical vein endothelial cells co-cultured with astrocytes from the same species (Figure 8 and S28). These models mimic the physical properties of the actual BBB in addition to showing low permeability values even for passively diffusing molecules (Figure S28B). According to a previous similar assay,[47] 8 h for the collection of samples showed to be a relevant timepoint. Kinetics studies are possible in this BBB model assay, but require to repeatedly take the cells out of the incubator. The change of temperature and atmosphere is detrimental to the stability of the barriers inducing a very significant increase in the barrier permeability. This would compromise determining the actual ability of the studied compound to cross the barrier. We decided to use the peptidomimetic in 1 mM concentration to warrant the detection after crossing the BBB model. Lower doses might have caused problems with the detection limit even when using highly sensitive methods like LC-MS-MS, leading to biased conclusions. The presented data were obtained from triplicates of two independent biological models using either human or mouse cells to establish the barriers. The outcome was comparable in these two models, with a low variability in the values among the triplicates, thus proving the significance of the results.

As shown in Figure 8, compound **7** is able to cross both murine and human BBB models, with a greater extent observed for the latter one. 8 h after addition of 1 mM dosage, $7 \pm 0.3\%$ of compound **7** had crossed the murine barrier, while $29 \pm 1.7\%$ were detected for the human barrier. This result demonstrated that peptidotriazolamers are able to cross the artificial human BBB to a higher extent than the murine one, thus making them a promising model for future design of drugs targeting the central nervous system.

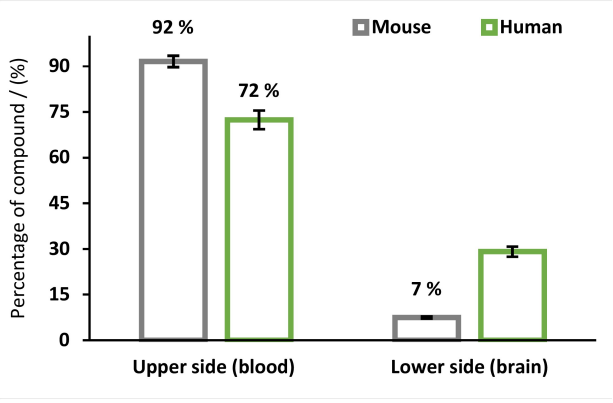

Figure 8. Passage of peptidotriazolamer **7** through the *in vitro* mouse (grey) and human (green) BBB at 8 h after addition of 1 mM dosage on the upper chamber. Data shown are means from three different triplicates ± SE.

Conclusion

We designed and synthesized peptidotriazolamers containing 1,4-disubstituted 1*H*-1,2,3-triazoles based on the two hot spot sequences $K^{16}LVFF^{20}$ and $G^{39}VVIA^{42}$ of Aβ(1–42) as parent peptides. The building block strategy of dipeptide mimetics by SPPS synthesis proved to be a versatile and adaptive method to prepare peptidomimetic foldamers characterized by synthetic monomers mimicking natural dipeptide side chains. By performing fluorescence assays and cell viability assays, we proved their ability in reducing the Aβ(1–42) oligomerization and the amount of soluble toxic oligomers formed. Peptidotriazolamer **7** was found to be an inhibitor with similar activity as its peptide counterpart and retained good inhibitory activity even at a substoichiometric ratio (**7**/Aβ(1–42) = 0.1 : 1). On the other hand, compound **6**, which differs from **7** only in the position of the triazole moieties, did not show any inhibition of oligomerization.

Conformational analyses by molecular dynamics simulations allowed to shed light on the differences in activity observed experimentally for compounds **2**, **6**, and **7** and on the related impact of the triazole positioning in the sequence. We demonstrated that peptidotriazolamer **7** can adopt an extended conformation like the parent peptide **2**, while peptidotriazolamer **6** folds in a "U"-shape. This different conformational behavior can be ascribed to the triazole positioning, which affects the global secondary structure of the pentapeptide sequence and thus its ability to disrupt the protein-protein interactions during the Aβ(1–42) oligomerization process.

In conclusion, we demonstrated the practical application of peptidomimetic foldamers in the area of therapeutics, particularly in pathologies involving abnormal protein-protein interactions. Peptidotriazolamers represent a new important class of peptidomimetic foldamers with biological activity. The further demonstration that this type of foldamers is also able to cross the *in vitro* BBB provides supporting data that peptidotriazolamers hold promise for the future design of drugs targeting the central nervous system.

Experimental Section

Synthesis of peptidotriazolamers

For the synthesis of the building blocks **20a–j** and all their intermediates, see the supporting information.

Resin was first swollen in DMF for 1 h in a reaction vessel equipped with a sintered glass bottom. Fmoc group on the linker was then removed by using a solution of 0.1 M HOBt and 20% piperidine in DMF (8 mL) for 40 min (deprotection cycle was performed twice). Subsequently, Fmoc protected amino acid or dipeptide triazolamer (building blocks **20a–j**) was first activated *in situ* by treatment with DIC (1.1 eq.) and Oxyma Plus (1.1 eq.) in DCM for 10 min and then transferred to the resin, dispersed in a solution of DMF (4 mL) and

2,4,6-trimethylpyridine (10 eq.). The amino acid or the building block (**20 a**–**j**) was then coupled by mechanical shaking at ambient temperature overnight. The coupling step was followed by a capping phase, using a solution of acetic anhydride (10 eq.) in DMF (8 mL) and stirring for one hour at ambient temperature. Successful completion of each coupling was monitored by UV spectroscopic method. The cycle of Fmoc removal and coupling was repeated with subsequent Fmoc protected amino acids or building blocks **20 a**–**j** to obtain resin-bound desired peptidotriazolamers (**3**–**7**). Each coupling was followed by removal of Fmoc, washing the resin by dimethylformamide (5×8 mL), dichloromethane (3×8 mL), methanol (1×8 mL), dichloromethane (1×8 mL) and dietylether (1×8 mL) and then drying. Cleavage of peptides from resin was carried out by using TFA:triisopropylsilane:water (95:2.5:2.5) as cleavage cocktail (10 mL), stirred by mechanical shaking at ambient temperature for 2 hours. Filtration afforded the peptidomimetic in filtrate which was evaporated under vacuum to remove the excess of TFA. Then, the crude was dissolved in ACN/water 1:1 (v/v) and freeze-dried, before performing the purification by HPLC (0%−70% of ACN/H_2O/TFA 95:5:0.1 in 45 min).

Fluorescence-detected Thioflavin-T binding assay

Stock solutions of compounds (**3**–**7**) were prepared in DMSO (20 mM). The Aβ(1–42) peptide was prepared in an aqueous 1% ammonia solution to a concentration of 1 mM and then, just prior to use, diluted to 0.2 mM with 10 mM Tris-HCl, 100 mM NaCl buffer (pH 7.4). Thioflavin T fluorescence was optimized to evaluate the development of Aβ(1–42) fibrils over time using a fluorescence plate reader (Fluostar Optima, BMG lab-tech) with standard 96-well black microtiter plates. The ThT fluorescence intensity was recorded with 440/480 nm excitation/emission filters set for 42 h applying a double orbital shaking of 10 s before the first cycle. Experiments were started by adding Aβ(1–42) reaching a final concentration of 10 μM into a mixture containing 40 μM Thioflavin T in 10 mM Tris-HCl, 100 mM NaCl buffer (pH 7.4) with and without the tested compounds at different concentrations (100, 10 and 1 μM) at 25 °C (maximal DMSO concentration of 0.5% (v/v)). Each condition was recorded in triplicate and the kinetic curve was fitted to a Boltzman sigmoidal equation using GraphPad Prism 7 from which the time of the half-life of aggregation ($t_{1/2}$) and the intensity of the experimental fluorescence plateau (*F*) were obtained. The ability of compounds to inhibit Aβ(1–42) aggregation was assessed considering both the $t_{1/2}$ extension/reduction and the *F* reduction. Refer to the Supporting Information for further details concerning the calculation of all the parameters.

Fluorescence-detected BODIPY binding assay

Stock solutions of the BODIPY dye for spectroscopic measurements and for time-dependent kinetics were prepared in EtOH (0.0428 mM) and subsequently diluted to 5.3 μM in PBS buffer (stock solution). The Aβ(1–42) peptide was dissolved during 15–20 minutes at room temperature in 0.16% NH_4OH solution at a peptide concentration of 2 mg/mL ans successively dried by immediate lyophilization. Then, the Aβ(1–42) peptide was reconstituted in 1% NH_4OH (at 1 mg/mL) with sonication at 25 °C for 1 minute before diluting in 20 mM phosphate buffer pH 7.4. Stock solutions of compounds (**3**–**7**) were prepared in DMSO (20 mM) and later diluted in PBS buffer to reach two different concentration (400 μM and 40 μM). BODIPY fluorescence was optimized to evaluate the development of Aβ(1–42) oligomers over time using a fluorescence plate reader (Tecan i-control 200) with standard 96-well black microtiter plates. The BODIPY fluorescence intensity was recorded with 518/540 nm excitation/emission filters set for 9 h performing a double orbital shaking of 10 s before the first cycle. Experiments were started by adding Aβ(1–42) to final concentration of 10 μM into a mixture containing 0.53 μM BODIPY in 20 mM buffer (pH 7.4) with and without the tested compounds at different concentrations (100 and 10 μM) at 25 °C. The kinetic curves are the representative average of triplicate measurements and representative values of two independent experiments. The ability of compounds to inhibit Aβ(1–42) aggregation is reported in Table 1 considering the time of the half-life of aggregation ($t_{1/2}$), the intensity of the experimental fluorescence plateau (*F*) and the slope of the linear part of the curve (first 4 hours). Refer to the Supporting Information for further details concerning the calculation of all the parameters.

Cell viability assay

SH-SY5Y neuroblastoma cells were grown in low serum Optimem (Life Technologies) for 24 h at 37 °C, 5% CO_2 in a 96 well plate at 20 000 cells per well. Aβ(1–42) was prepared according to the oligomerization protocol B (see the Supporting Information). The Aβ(1–42) aliquot was prepared by dissolving in sterile PBS (20 mM phosphate buffer pH 7.4) reaching a final Aβ(1–42) concentration of 50 μM in the presence of 250 and 50 μM of compound **5** and of 50 and 5 μM of compound **7** for 24 h at 37 °C, along with a negative control without inhibitor and a positive control with Ac-GVVIA-NH_2 (250 and 50 μM). After the 24 h period, media was removed from the cells and replaced with Optimem containing the preincubated Aβ(1–42) solutions diluted one to ten (5 μM Aβ(1–42) final concentration). The cells were incubated for a further 24 hours. The cell viability (MTS assay) was performed using the Cell Titer 96® Aqueous One Solution Cell Proliferation Assay (Promega). The assay was performed in two independent experiments with $n = 6$ for each condition. The significant difference between the values from cells in the presence of Aβ(1–42) and cells in the presence of Aβ(1–42) and the inhibitor ($p < 0.05$, 0.01, and 0.001) was measured by statistical ANOVA test.

Conformational analysis

Molecular Dynamics (MD) simulations were conducted using the Amber20 modelling software suite and the specially tailored TZLff molecular mechanics force-field parametrization for peptidotriazolamers.[44,48] Initial 100 independent simulated annealing MD runs in gas phase with NMR derived distance restraints served as input for the subsequent MD simulation in explicit DMSO environment as well as TIP4Pew water. After energy minimization and heat-up of the solvated system, three parallel 200 ns MD production runs for each molecule and solvent were performed at 300 K. All non-time dependent analyses were performed on merged replica data over the last half of each trajectory. Time series were analyzed for each replicate individually for the whole trajectory length. Further details regarding the methodology can be found in the Supporting Information.

In vitro blood-brain barrier permeability measurements

In vitro mouse and human BBB inserts were prepared as described by Le Joncour et al.[46] Briefly, human BBB is induced by co-culturing immortalized HuAR2T endothelial cells[49] with normal human astrocytes (Lonza, CC-2565) for 7 days. Mouse BBB is obtained by co-culturing the brain microvessel endothelial cell line (bEND3)[50] with HIFko mouse astrocytes for 5 days.[51] As described in Le Joncour *et al.*[46] and in Fig. S28 A (SI), assay quality verification is performed before testing the molecule of interest. Briefly, once the optimal co-culture incubation duration for establishing the barriers

is reached, one randomly selected insert is used to calculate the barrier permeability. Sodium fluorescein is added to the "blood" side of the chamber and samples from the "brain" side are collected at several timepoints. Permeability is calculated using the following formula after measuring the fluorescence intensities from both "blood" and "brain" samples using a fluorescence plate reader: permeability = dQ/(dT*A*C0), with dQ the fluorescence intensity from the "brain" side, dT the timepoint in s, A the surface of the insert in cm^2 and C0 the initial fluorescence intensity from the "blood" side. If the permeability is $< 10 \times 10^{-5}$ cm/s, the inserts are used to proceed further with the experiment. The medium from the inserts (e.g. endothelial/"blood" side) is replaced by fresh endothelial cell culture medium containing the tested compound **7** (1 mM, n = 3). Controls were incubated with the same medium devoid of any test compound. The inserts were then incubated for 8 h at 37 °C. Eventually, cell culture medium samples were collected from both the "blood" and "brain" sides of each chamber. Passage of the compound **7** from the blood to the brain side has been determined by mass spectrometry. For details concerning the LC-MS quantification, refer to the Supporting Information.

Acknowledgements

We acknowledge Carmela Michalek for the cell viability assay. The authors gratefully thank the de.NBI Cloud Team for the access to the BMBF-funded de.NBI Cloud within the German Network for Bioinformatics Infrastructure (de.NBI) (031A537B, 031A533A, 031A538A, 031A533B, 031A535A, 031A537C, 031A534A, 031A532B) as the major computational resource for this project. The authors also acknowledge the support of TUBITAK ULAKBIM High Performance and Grid Computing Center (TRUBA resources) for additional calculations. Open access funding enabled and organized by Projekt DEAL.

Conflict of Interest

The authors declare no conflict of interest.

Keywords: αβ oligomerization inhibitors · amyloids · foldamers · peptidomimetics · peptidotriazolamers

[1] M. Ankarcrona, B. Winblad, C. Monteiro, C. Fearns, E. T. Powers, J. Johansson, G. T. Westermark, J. Presto, B.-G. Ericzon, J. W. Kelly, *J. Intern. Med.* **2016**, *280*, 177–202.
[2] L. C. dos Santos Picanco, P. F. Ozela, M. de Fatima de Brito Brito, A. A. Pinheiro, E. C. Padilha, F. S. Braga, C. H. T. de Paula da Silva, C. B. R. dos Santos, J. M. C. Rosa, L. I. da Silva Hage-Melim, *Curr. Med. Chem.* **2018**, *25*, 3141–3159.
[3] *Alzheimer's Dementia* **2020**, *16*, 391–460.
[4] T. Mohamed, A. Shakeri, P. P. N. Rao, *Eur. J. Med. Chem.* **2016**, *113*, 258–272.
[5] M. A. Busche, B. T. Hyman, *Nat. Neurosci.* **2020**, *23*, 1183–1193.
[6] W. Jagust, *Nat. Rev. Neurosci.* **2018**, *19*, 687–700.
[7] X. Du, X. Wang, M. Geng, *Transl. Neurodegener.* **2018**, *7*, DOI 10.1186/s40035-018-0107-y.
[8] J. Cao, J. Hou, J. Ping, D. Cai, *Mol. Neurodegener.* **2018**, *13*, 64.
[9] J. L. Cummings, T. Morstorf, K. Zhong, *Alzheimers Res. Ther.* **2014**, *6*, 37.
[10] S. Salloway, R. Sperling, N. C. Fox, K. Blennow, W. Klunk, M. Raskind, M. Sabbagh, L. S. Honig, A. P. Porsteinsson, S. Ferris, M. Reichert, N. Ketter, B. Nejadnik, V. Guenzler, M. Miloslavsky, D. Wang, Y. Lu, J. Lull, I. C. Tudor, E. Liu, M. Grundman, E. Yuen, R. Black, H. R. Brashear, *N. Engl. J. Med.* **2014**, *370*, 322–333.
[11] A. E. Oxford, E. S. Stewart, T. T. Rohn, *Int. J. Alzheimers Dis.* **2020**, *2020*, DOI 10.1155/2020/5380346.
[12] X.-Q. Chen, W. C. Mobley, *Front. Neurosci.* **2019**, *13*, DOI 10.3389/fnins.2019.00659.
[13] I. C. Fontana, A. R. Zimmer, A. S. Rocha, G. Gosmann, D. O. Souza, M. V. Lourenco, S. T. Ferreira, E. R. Zimmer, *J. Neurochem.* **2020**, 155, 348–369.
[14] Y. Huang, R. Liu, *Int. J. Mol. Sci.* **2020**, *21*, 4477.
[15] J. Fantini, H. Chahinian, N. Yahi, *Protein Sci.* **2020**, *29*, 1748–1759.
[16] C. Nerelius, A. Sandegren, H. Sargsyan, R. Raunak, H. Leijonmarck, U. Chatterjee, A. Fisahn, S. Imarisio, D. A. Lomas, D. C. Crowther, R. Strömberg, J. Johansson, *Proc. Mont. Acad. Sci.* **2009**, *106*, 9191–9196.
[17] N. Tonali, V. I. Dodero, J. Kaffy, L. Hericks, S. Ongeri, N. Sewald, *ChemBioChem* **2020**, *21*, 1129–1135.
[18] N. Tonali, J. Kaffy, J.-L. Soulier, M. L. Gelmi, E. Erba, M. Taverna, C. van Heijenoort, T. Ha-Duong, S. Ongeri, *Eur. J. Med. Chem.* **2018**, *154*, 280–293.
[19] S. Pellegrino, N. Tonali, E. Erba, J. Kaffy, M. Taverna, A. Contini, M. Taylor, D. Allsop, M. L. Gelmi, S. Ongeri, *Chem. Sci.* **2017**, *8*, 1295–1302.
[20] J. Kaffy, D. Brinet, J.-L. Soulier, I. Correia, N. Tonali, K. F. Fera, Y. Iacone, A. R. F. Hoffmann, L. Khemtémourian, B. Crousse, M. Taylor, D. Allsop, M. Taverna, O. Lequin, S. Ongeri, *J. Med. Chem.* **2016**, *59*, 2025–2040.
[21] S. Giorgetti, C. Greco, P. Tortora, F. A. Aprile, *Int. J. Mol. Sci.* **2018**, *19*, 2677.
[22] J. Renaud, M.-G. Martinoli, *Int. J. Mol. Sci.* **2019**, *20*, 1883.
[23] X. Ran, J. E. Gestwicki, *Curr. Opin. Chem. Biol.* **2018**, *44*, 75–86.
[24] https://www.neurimmune.com/news/neurimmune-welcomes-biogens-news-on-european-medicines-agency-acceptance-of-the-marketing-authorization-application-for-aducanumab, **2020**.
[25] https://www.ema.europa.eu/en/medicines/medicines-under-evaluation, **2020**.
[26] P. Chames, M. Van Regenmortel, E. Weiss, D. Baty, *Br. J. Pharmacol.* **2009**, *157*, 220–233.
[27] L. Nevola, E. Giralt, *Chem. Commun.* **2015**, *51*, 3302–3315.
[28] J. L. Lau, M. K. Dunn, *Bioorg. Med. Chem.* **2018**, *26*, 2700–2707.
[29] R. Gopalakrishnan, A. I. Frolov, L. Knerr, W. J. Drury, E. Valeur, *J. Med. Chem.* **2016**, *59*, 9599–9621.
[30] G. Guichard, I. Huc, *Chem. Commun.* **2011**, *47*, 5933–5941.
[31] A. Trabocchi, A. Guarna, *Peptidomimetics in Organic and Medicinal Chemistry*, John Wiley & Sons, Ltd, Chichester, **2014**, Chapter 10, pp. 219–229.
[32] T. A. Martinek, F. Fülöp, *Chem. Soc. Rev.* **2012**, *41*, 687–702.
[33] J. Laxio Arenas, J. Kaffy, S. Ongeri, *Curr. Opin. Chem. Biol.* **2019**, *52*, 157–167.
[34] L. Vahdati, J. Kaffy, D. Brinet, G. Bernadat, I. Correia, S. Panzeri, R. Fanelli, O. Lequin, M. Taverna, S. Ongeri, U. Piarulli, *Eur. J. Org. Chem.* **2017**, *2017*, 2971–2980.
[35] J. Kaffy, C. Berardet, L. Mathieu, B. Legrand, M. Taverna, F. Halgand, G. Van Der Rest, L. T. Maillard, S. Ongeri, *Chem. Eur. J.* **2020**, *26*, 14612–14622.
[36] N. G. Angelo, P. S. Arora, *J. Am. Chem. Soc.* **2005**, *127*, 17134–17135.
[37] O. Kracker, J. Góra, J. Krzciuk-Gula, A. Marion, B. Neumann, H.-G. Stammler, A. Nieß, I. Antes, R. Latajka, N. Sewald, *Chem. Eur. J.* **2018**, *24*, 953–961.
[38] D. C. Schröder, O. Kracker, T. Fröhr, J. Góra, M. Jewginski, A. Nieß, I. Antes, R. Latajka, A. Marion, N. Sewald, *Front. Chem.* **2019**, *7*, 155.
[39] J. R. Johansson, E. Hermansson, B. Nordén, N. Kann, T. Beke-Somfai, *Eur. J. Org. Chem.* **2014**, *2014*, 2703–2713.
[40] O. Kracker, *PhD Thesis*, Bielefeld University, **2019**.
[41] Lundquist, J. C. Pelletier, *Org. Lett.* **2001**, *3*, 781–783.
[42] M. Wünsch, D. Schröder, T. Fröhr, L. Teichmann, S. Hedwig, N. Janson, C. Belu, J. Simon, S. Heidemeyer, P. Holtkamp, J. Rudlof, L. Klemme, A. Hinzmann, B. Neumann, H.-G. Stammler, N. Sewald, *Beilstein J. Org. Chem.* **2017**, *13*, 2428–2441.
[43] P. B. Alper, S.-C. Hung, C.-H. Wong, *Tetrahedron Lett.* **1996**, *37*, 6029–6032.
[44] A. Marion, J. Góra, O. Kracker, T. Fröhr, R. Latajka, N. Sewald, I. Antes, *J. Chem. Inf. Model.* **2018**, *58*, 90–110.
[45] L. Tran, N. Basdevant, C. Prévost, T. Ha-Duong, *Sci. Rep.* **2016**, *6*, 21429.
[46] V. Le Joncour, S. Karaman, P. M. Laakkonen, *J. Visualization* **2019**, *146*, e59384.
[47] J. Merisaari, O. V. Denisova, M. Doroszko, V. Le Joncour, P. Johansson, W. P. J. Leenders, D. B. Kastrinsky, N. Zaware, G. Narla, P. Laakkonen, S.

Nelander, M. Ohlmeyer, J. Westermarck, *Brain Commun.* **2020**, *2(1)*, fcaa002.
[48] D. A. Case, K. Belfon, I. Y. Ben-Shalom, S. R. Brozell, D. S. Cerutti, T. E. Cheatham, III, V. W. D. Cruzeiro, T. A. Darden, R. E. Duke, G. Giambasu, M. K. Gilson, H. Gohlke, A. W. Goetz, R. Harris, S. Izadi, S. A. Izmailov, K. Kasavajhala, A. Kovalenko, R. Krasny, T. Kurtzman, T. S. Lee, S. LeGrand, P. Li, C. Lin, J. Liu, T. Luchko, R. Luo, V. Man, K. M. Merz, Y. Miao, O. Mikhailovskii, G. Monard, H. Nguyen, A. Onufriev, F. Pan, S. Pantano, R. Qi, D. R. Roe, A. Roitberg, C. Sagui, S. Schott-Verdugo, J. Shen, C. L. Simmerling, N. R. Skrynnikov, J. Smith, J. Swails, R. C. Walker, J. Wang, L. Wilson, R. M. Wolf, X. Wu, Y. Xiong, Y. Xue, D. M. York, P. A. Kollman, *AMBER 2020*, University of California, San Francisco, **2020**.
[49] T. May, M. Butueva, S. Bantner, D. Markusic, J. Seppen, R. A. F. MacLeod, H. Weich, H. Hauser, D. Wirth, *Tissue Eng. Part A* **2009**, *16*, 441–452.
[50] S. Yang, S. Mei, H. Jin, B. Zhu, Y. Tian, J. Huo, X. Cui, A. Guo, Z. Zhao, *PLoS One* **2017**, *12*, e0187017.
[51] B. Blouw, H. Song, T. Tihan, J. Bosze, N. Ferrara, H.-P. Gerber, R. S. Johnson, G. Bergers, *Cancer Cell* **2003**, *4*, 133–146.

Manuscript received: December 23, 2020
Revised manuscript received: April 7, 2021
Accepted manuscript online: April 8, 2021